Inorganic Chemistry

Article

pubs.acs.org/IC

Free Base and Metal Complexes of 5,15-Diaza-10,20-dimesitylporphyrins: Synthesis, Structures, Optical and Electrochemical Properties, and Aromaticities

Yoshihiro Matano,*[,†] Tarou Shibano,[†] Haruyuki Nakano,[‡] Yoshifumi Kimura,[§] and Hiroshi Imahori[†,∥]

[†]Department of Molecular Engineering, Graduate School of Engineering, Kyoto University, Nishikyo-ku, Kyoto 615-8510, Japan

[‡]Department of Chemistry, Graduate School of Sciences, Kyushu University, Fukuoka 812-8581, Japan

[§]Department of Chemical Science and Technology, Faculty of Bioscience and Applied Chemistry, Hosei University, Tokyo 184-8584, Japan

[∥]Institute for Integrated Cell-Material Sciences (WPI-iCeMS), Kyoto University, Nishikyo-ku, Kyoto 615-8510, Japan

Supporting Information

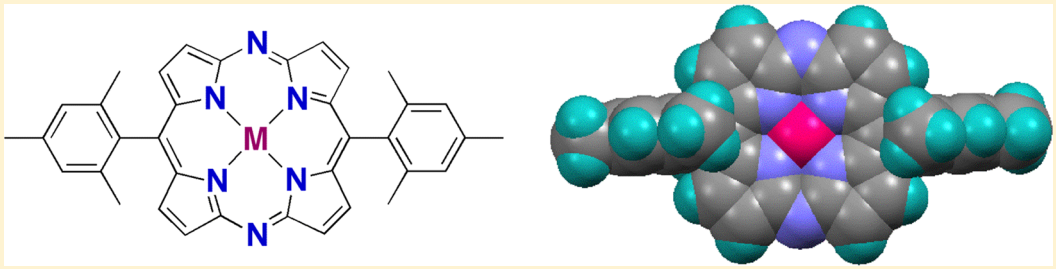

ABSTRACT: The synthesis, structures, optical and electrochemical properties, and aromaticity of a series of 5,15-diaza-10,20-dimesitylporphyrins (M−DAP; M = Pb, H_2, Ni, Pd, Pt, Zn; mesityl = 2,4,6-trimethylphenyl) are reported. Treatment of mesityl-substituted bis(5,5′-dibromodipyrrin) with sodium azide in the presence of lead(II) acetylacetonate afforded Pb−DAP, which was quantitatively converted to H_2−DAP by acidolysis. The free base H_2−DAP reacted with palladium(II), platinum(II), and zinc(II) salts to give Pd−DAP, Pt−DAP, and Zn−DAP, respectively. The crystal structures, optical and electrochemical properties, and aromaticities of these β-unsubstituted M−DAPs were comprehensively investigated by X-ray crystallography, UV−vis absorption/fluorescence spectroscopy, nanosecond flash photolysis, cyclic and differential pulse voltammetry, NMR spectroscopy, and density functional theory calculations. The obtained data show that replacement of the 5- and 15-methine carbons with nitrogen atoms alters the intrinsic properties of the porphyrin 18π system as follows: (i) the coordination spheres at the N_4 core become contracted while keeping high planarity; (ii) the Q bands are red shifted and largely intensified; (iii) the electron-accepting ability is enhanced, whereas the electron-donating ability is reduced; (iv) the radiative decay rates from the S_1 state are enhanced; and (v) the aromaticity of the 18π circuit is slightly reduced in terms of both geometric and magnetic criteria. These optical and electrochemical properties of M−DAPs stem from their characteristic frontier orbitals; two HOMOs and two LUMOs are nondegenerate as a result of the incorporation of the electronegative nitrogen atoms at the two meso positions. In addition, the group 10 metals incorporated at the core finely tune the fundamental properties of DAP π systems through inductive effects as well as dπ−pπ antibonding orbital interactions; the HOMO−LUMO gaps of the group 10 metal complexes increase in the order Ni−DAP < Pd−DAP < Pt−DAP.

INTRODUCTION

5,15-Diazaporphyrins (DAPs) are a class of azaporphyrins that bear two meso-nitrogen atoms linking two dipyrromethene (dipyrrin) units. Since Fischer and co-workers reported the first example in 1936,[1] DAPs have received continuing interest in relation to their parent tetrapyrrole macrocycles, porphyrins, and tetraazaporphyrins.[2] For example, Kobayashi, Neya, Stuzhin, and co-workers extensively investigated the effects of the replacement of 5- and 15-methine carbons with nitrogen atoms (5,15-aza-substitution) on the optical and electrochemical properties of the 2,3,7,8,12,13,17,18-octaalkylporphyrin π systems by comparing M−DAP (**P1** in Chart 1; M = Cu, H_2) with the corresponding porphyrins.[3] It has been shown that 5,15-aza-substitution significantly changes the intrinsic properties of the porphyrin π systems. In the fields of coordination and materials chemistry, DAPs have been used as redox-active and photoactive macrocyclic N_4-ligands like porphyrins and phthalocyanines.[4,5] For example, Fe−DAPs (**P1**; M = FeL; L = axial ligand) were used to examine novel biological aspects of myoglobin[6] and low-spin states of isocyanide-bound model hemes,[7] and Zn−DAP (**P1**; M = Zn, 2H, R = Me, R′ = C_6H_{13}) and Cu−DAP (**P2**; M = Cu, R = H)

Received: August 22, 2012
Published: November 8, 2012

Chart 1

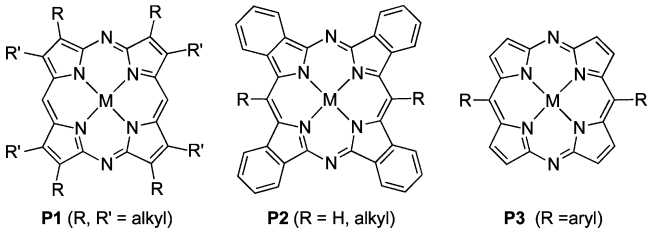

have been used as singlet-oxygen generators[8,9] and a p-type field-effect transistor,[10] respectively. In addition, multiply metal-linked DAP architectures such as sandwich-type homoleptic lanthanide triple-deckers,[11] heteroleptic cerium double-deckers,[12] and a linear-type externally Pd-coordinated trimer[13] have been constructed and their spectral properties described. Despite having these intriguing properties, however, the number of metal complexes of DAP is still limited compared with those of porphyrins and phthalocyanines. It is therefore of significance to reveal the structure−property relationships of a series of metal complexes bearing identical DAP ligands.

Most DAPs are fully substituted at the pyrrolic β-carbons (**P1** and **P2** in Chart 1) and have been prepared from dibromodipyrrins, isoindoline-1,3-diimine, or their synthons.[14,15] In contrast, the literature contains very few examples of β-unsubstituted DAP derivatives (**P3** in Chart 1).[16] We thought that this class of compounds would be a promising platform for development of diazaporphyrin-based materials and catalysts, because various substituents can be introduced to the peripheral β-carbons from the common DAP skeletons. Quite recently, we reported the first comprehensive study of β-unsubstituted DAP−metal complexes, Ni−DAP (**2Ni**) and Cu−DAP (**2Cu**), both of which were successfully prepared from the β-unsubstituted bis(5,5′-dibromodipyrrin)−metal complexes **1M** (M = Ni, Cu) using a metal-template method (Scheme 1).[17,18] It has been revealed that

Scheme 1. Metal-Template Synthesis of 2Ni and 2Cu

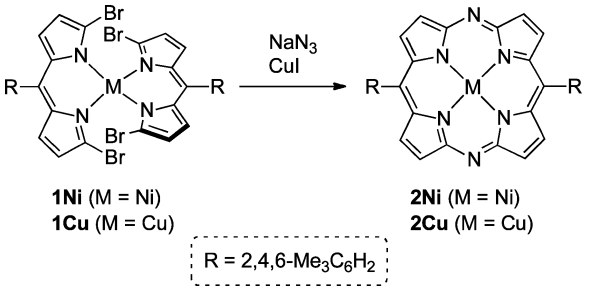

the optical and electrochemical properties of **2Ni** are different from those of a nickel porphyrin reference. Furthermore, we established a convenient method for the regioselective functionalization of the β-carbons of **2Ni** with phenyl groups based on a bromination−cross-coupling strategy. As expected, the introduced phenyl groups considerably altered the HOMO−LUMO gap of the D_{2h}-symmetric M−DAP π system through effective π conjugation. These results prompted us to investigate the chemistry of a new series of β-unsubstituted DAP−metal complexes and compare their properties.

In this paper, we report the synthesis, structures, optical and electrochemical properties, and aromaticities of free base and metal complexes of 5,15-diaza-10,20-dimesitylporphyrin (M−DAP; M = H_2, Pb, Ni, Pd, Pt, Zn; mesityl =2,4,6-trimethylphenyl). Various experimental techniques, including X-ray crystallography, NMR spectroscopy, steady-state absorption/emission spectroscopy, nanosecond flash photolysis, and cyclic/differential pulse voltammetry, were used to elucidate the effects of meso nitrogen atoms and central metals on the fundamental properties of the M−DAP π systems. Density functional theory (DFT) and time-dependent DFT (TD-DFT) calculations on M−DAP and porphyrin models were also performed to understand the nature of the frontier orbitals and the electronic excitations of the β-unsubstituted M−DAP π systems.

RESULTS AND DISCUSSION

Synthesis and Characterization. We first attempted to synthesize a zinc complex of 5,15-diaza-10,20-dimesitylporphyrin (Zn−DAP; **2Zn**) using the metal-template method. Treatment of mesityl-substituted 5,5′-dibromodipyrrin **3**[17] with $Zn(OAc)_2$ proceeded smoothly to give bis(5,5′-dibromodipyrrin)−zinc(II) complex **1Zn** (Scheme 2), which was characterized by NMR spectroscopy, mass spectrometry, and X-ray crystallography.

Scheme 2. Synthesis of 1Zn

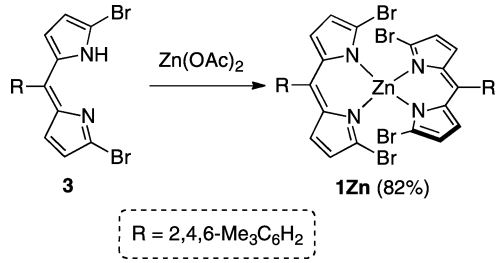

As shown in Figure 1, the zinc center in **1Zn** adopts a distorted tetrahedral geometry with Zn−N bond lengths of

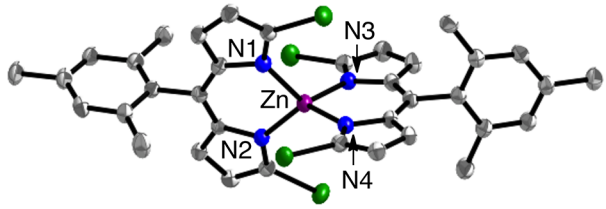

Figure 1. Crystal structure of **1Zn** (30% probability ellipsoids). Hydrogen atoms are omitted for clarity: gray (C), blue (N), purple (Zn). Selected bond lengths (Angstroms) and angles (degrees): Zn−N1, 1.974(5); Zn−N2, 1.976(4); Zn−N3, 1.990(5); Zn−N4, 1.975(5); N1−Zn−N2, 94.95(19); N1−Zn−N3, 117.98(19); N1−Zn−N4, 113.76(19); N2−Zn−N3, 111.87(19); N2−Zn−N4, 125.44(19); N3−Zn−N4, 94.7(2).

1.974(5)−1.990(5) Å and endocyclic N−Zn−N bond angles of 94.7(2)−94.95(19)°. The dihedral angle between the two N−Zn−N planes of **1Zn** (82.9°) is very close to that of a 5,5′-unsubstituted analog (83.4°) reported by Maeda and co-workers.[19] Presumably, the d^{10} zinc(II) center in the bis(dibromodipyrrin) complexes essentially prefers to adopt a tetrahedral geometry.

Aza-annulation of **1Zn** was conducted using NaN_3−CuI in DMF, which was effective for the synthesis of **2Ni** and **2Cu**. Although TLC analysis of the reaction mixture suggested formation of a trace amount of **2Zn**, it could not be isolated in acceptable yield. We therefore decided to prepare metal complexes other than **2Ni** and **2Cu** via a free base (H_2−DAP; $\mathbf{2H_2}$).

dx.doi.org/10.1021/ic301835c | Inorg. Chem. 2012, 51, 12879−12890

Scheme 3 depicts the synthesis of $2H_2$, which is based on Stuzhin's lead-template method.[20,21]

Scheme 3. Synthesis of 2Pb and $2H_2$

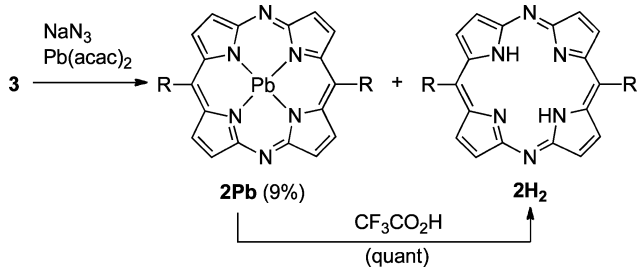

Treatment of **3** with NaN_3 in the presence of $Pb(acac)_2$ in refluxing MeOH afforded Pb–DAP (**2Pb**) as a green solid in 9% isolated yield together with a trace amount of H_2–DAP ($2H_2$).[22] The structures of **2Pb** and $2H_2$ were characterized on the basis of spectral and X-ray crystallographic data (vide infra). Our present results contrast with Stuzhin's results on the synthesis of β-substituted DAP derivatives[20] in that the lead(II) complex **2Pb** was isolated as the major product. It should be noted that **2Pb** was quantitatively converted to the free base $2H_2$ by treatment with trifluoroacetic acid at room temperature. The lead-assisted aza-annulation of **3** was therefore applicable to the synthesis of $2H_2$.

With $2H_2$ in hand, Pd–DAP (**2Pd**), Pt–DAP (**2Pt**), and Zn–DAP (**2Zn**) were successfully prepared by complexation with the corresponding metal(II) salts in 89%, 54%, and 93% yields, respectively (Scheme 4). Except for **2Zn**, the metal

Scheme 4. Synthesis of 2Pd, 2Pt, and 2Zn

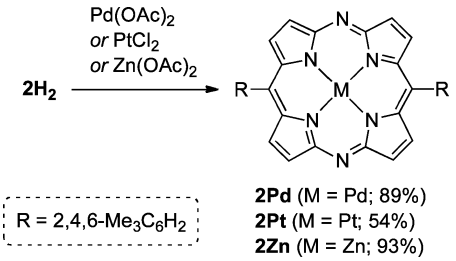

complexes and free base (**2M**; M = Pb, H_2, Ni, Pd, Pt) are easily soluble in CH_2Cl_2. The zinc complex **2Zn** is sparingly soluble in CH_2Cl_2 and moderately soluble in a CH_2Cl_2–MeOH mixed solvent at room temperature, suggesting that **2Zn** self-aggregates in CH_2Cl_2.

The new β-unsubstituted M–DAPs **2M** (M = H_2, Pb, Pd, Pt, Zn) were characterized using conventional spectroscopic techniques, including NMR spectroscopy and mass spectrometry. In the ^{1}H NMR spectra of $2H_2$, **2Pd**, **2Pt**, and **2Zn**, two kinds of pyrrolic β-protons appeared at δ 8.70–8.84 and 9.08–9.24 ppm (each d, 4H) and the ortho methyl and meta protons of the mesityl groups were observed to be equivalent, indicating that these M–DAPs possess high symmetry on average in solution. In contrast, in the ^{1}H NMR spectrum of **2Pb**, the ortho methyl and meta protons of the mesityl groups were not equivalent. As the covalent bond radius of lead is relatively long compared with the covalent bond radii of the group 10 metals,[23] the lead atom in **2Pb** is likely to deviate from the DAP π plane as observed for β-substituted DAP–indium(III) complexes.[24] The pyrrolic NH protons of $2H_2$ and 5,15-dimesitylporphyrin ($4H_2$)[25] appeared at δ = −2.61 and −3.12 ppm, respectively; this shows that the magnetic shielding effects at the core of the diazaporphyrin ring in $2H_2$ are smaller than that of the porphyrin ring in $4H_2$. Similarly, the magnetic deshielding effects on the pyrrolic β-protons of $2H_2$ (δ 8.84 and 9.24 ppm) and **2Zn** (δ 8.78 and 9.15 ppm) are slightly smaller than those of $4H_2$ (δ 8.85 and 9.36 ppm) and **4Zn**[25] (δ 8.93 and 9.41 ppm). Overall, the aromaticity of **2M** is somewhat weaker than that of **4M** in terms of magnetic criteria (vide infra).

Crystal Structures. The crystal structures of $2H_2$, **2Pd**, **2Pt**, and 5,15-dimesitylporphyrinatonickel (**4Ni**) were elucidated by X-ray crystallography (Figures 2–4 and Figure S1 in

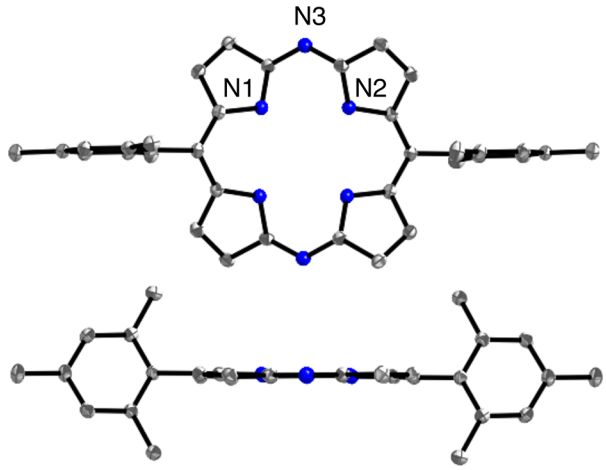

Figure 2. Crystal structure of $2H_2$ (30% probability ellipsoids): Top view (top) and side view (bottom). Hydrogen atoms are omitted for clarity: gray (C), blue (N). d_{RMS} = 0.023 Å.

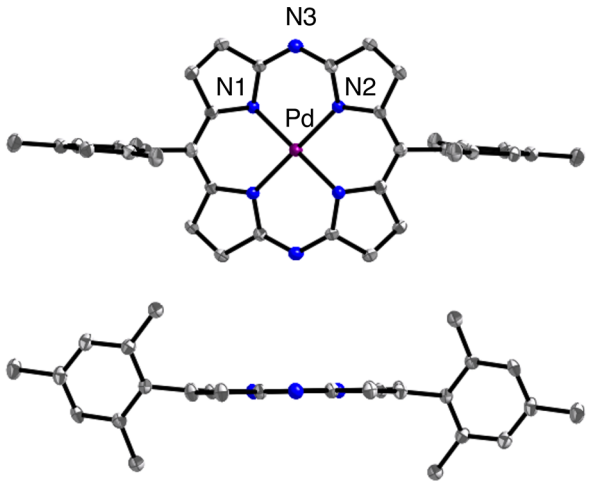

Figure 3. Crystal structure of **2Pd** (30% probability ellipsoids): Top view (top) and side view (bottom). Hydrogen atoms are omitted for clarity: gray (C), blue (N), purple (Pd). d_{RMS} = 0.017 Å.

Supporting Information).[26] Bond lengths, bond angles, and dihedral angles are summarized in Table 1, together with the data for **2Ni**.[17] The deviations of the 24 C/N DAP-ring atoms from the mean DAP π plane (d in Angstroms) are listed in Figure S2 in the Supporting Information. In all compounds characterized, the meso mesityl groups are almost perpendicular to the DAP π planes, with dihedral angles of 84.1–87.3°.

dx.doi.org/10.1021/ic301835c | Inorg. Chem. 2012, 51, 12879–12890

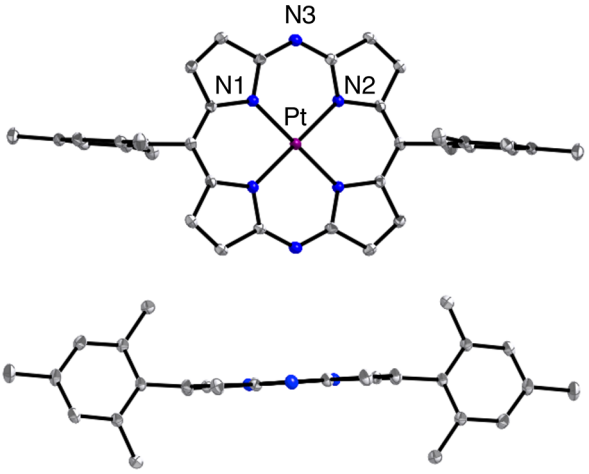

Figure 4. Crystal structure of **2Pt** (30% probability ellipsoids): Top view (top) and side view (bottom). Hydrogen atoms are omitted for clarity: gray (C), blue (N), purple (Pt). d_{RMS} = 0.016 Å.

As shown in Figure 2, the free base **2H$_2$** has a highly planar π plane with a small root-mean-square (RMS) d value (d_{RMS}, 0.023 Å). The N1···N2 distances in **2H$_2$** (2.80−2.83 Å) are appreciably longer than those in **2Ni** (2.69−2.72 Å). In addition, the N(*meso*)−N(*meso*)′ and C(*meso*)−C(*meso*)′ distances in **2H$_2$** (6.80 and 6.82 Å) are also longer than the respective values in **2Ni** (6.77 and 6.78 Å). Obviously, insertion of nickel(II) contracts the DAP π system through formation of the four Ni−N bonds at the core.

As shown in Figures 3 and 4, the metal centers in **2Pd** and **2Pt** adopt a square-planar geometry (Σ_{N-M-N} = 360°) like that of the nickel center in **2Ni**. The M−N bond lengths of these group 10 complexes are 1.913(2)−1.915(2) Å for **2Ni**, 1.979(3)−1.989(3) Å for **2Pd**, and 1.984(2)−1.985(2) Å for **2Pt**, which reflects the covalent radii of the respective group 10 metals.[23] The d_{RMS} values of **2Ni**, **2Pd**, and **2Pt** are 0.018, 0.017, and 0.016 Å, respectively, indicating that their DAP π planes are highly planar. The difference in the M−N bond lengths is mainly reflected in difference in the C−N(*meso*)−C and C−C(*meso*)−C bond angles (α and β in Table 1); these values become wider going down the group 10 column.

The Ni−N bond lengths of **2Ni** [1.913(2)−1.915(2) Å] are shorter than those of **4Ni** [1.950(2)−1.955(2) Å], indicating that the core size of **2Ni** is appreciably smaller than that of **4Ni**. 5,15-Aza-substitution of the porphyrin ligand mainly induces structural changes at the two meso nitrogen bridges; the N(*meso*)−C bond lengths of **2Ni** [*a*, *a*′ in Table 1; 1.321(3)−1.325(3) Å] are shorter than the corresponding C(*meso*)−C bond lengths of **4Ni** [*a*, *a*′; 1.369(3)−1.372(3) Å], and the C−N(*meso*)−C bond angle of **2Ni** [α in Table 1; 120.14(18)°] is narrower than the corresponding C−C(*meso*)−C bond angle of

Table 1. Bond Lengths and Distances, Bond Angles, and Dihedral Angles of 2M and 4Ni

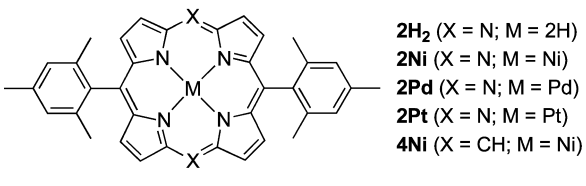

2H$_2$ (X = N; M = 2H)
2Ni (X = N; M = Ni)
2Pd (X = N; M = Pd)
2Pt (X = N; M = Pt)
4Ni (X = CH; M = Ni)

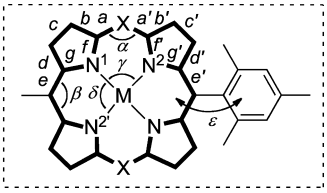

	2H$_2$	2Ni	2Pd	2Pt	4Ni
bond lengths/distances (Å)					
a	1.334(3)	1.321(3)	1.342(4)	1.327(3)	1.369(3)
a′	1.327(3)	1.325(3)	1.327(4)	1.322(3)	1.372(3)
b	1.450(3)	1.438(3)	1.421(4)	1.438(4)	1.428(3)
b′	1.437(3)	1.442(3)	1.445(4)	1.438(4)	1.431(3)
c	1.339(3)	1.341(3)	1.343(4)	1.341(4)	1.345(3)
c′	1.354(3)	1.345(3)	1.337(5)	1.342(4)	1.343(3)
d	1.452(3)	1.441(3)	1.449(4)	1.447(4)	1.436(3)
d′	1.430(3)	1.441(3)	1.442(4)	1.443(4)	1.445(3)
e	1.394(3)	1.380(3)	1.393(4)	1.395(4)	1.381(3)
e′	1.396(3)	1.386(3)	1.395(4)	1.387(4)	1.378(3)
f	1.359(3)	1.376(3)	1.366(4)	1.372(3)	1.384(2)
f′	1.367(3)	1.380(2)	1.356(4)	1.379(3)	1.380(2)
g	1.373(2)	1.384(2)	1.368(4)	1.375(3)	1.388(2)
g′	1.375(2)	1.383(2)	1.370(4)	1.374(3)	1.384(2)
M−N^1		1.913(2)	1.979(3)	1.984(2)	1.950(2)
M−N^2		1.915(2)	1.989(3)	1.985(2)	1.955(2)
N^1···N^2	2.80	2.69	2.80	2.80	2.78
N^1···N$^{2\prime}$	2.83	2.72	2.82	2.82	2.74
bond angles (degrees)					
α	122.51(18)	120.14(18)	122.6(3)	123.5(2)	124.22(19)
β	124.48(18)	122.04(18)	123.6(3)	124.3(2)	121.82(18)
γ		89.33(7)	89.58(11)	89.63(8)	90.90(7)
δ		90.67(7)	90.42(11)	90.37(8)	89.10(7)
dihedral angles (degrees)					
ε	87.3	86.2	87.1	87.7	80.0

dx.doi.org/10.1021/ic301835c | *Inorg. Chem.* 2012, 51, 12879−12890

4Ni [α; 124.22(19)°]. It is now evident that the β-unsubstituted DAP ligand finely tunes its coordination sphere to keep the high planarity of the π plane.

Optical and Electrochemical Properties. To investigate the optical and electrochemical properties of the β-unsubstituted M–DAP derivatives in comparison with those of porphyrin references, we measured the UV–vis absorption spectra and redox potentials of **2M** and **4M**[27] in solution (Tables 2 and 3).

Table 2. UV–vis Absorption Data for 2M and 4M

compound	λ_{max}/nm[a]
2H$_2$	393, 541, 627
2Pb	334, 459, 595, 618
2Ni[b]	373, 390, 571
2Pd	394, 564
2Pt	383, 557
2Zn[c]	394, 552, 584
4H$_2$	403, 500, 534, 572, 627
4Ni[b]	398, 514, 547
4Zn	409, 538, 573

[a]Measured in CH_2Cl_2 except for **2Zn**. [b]Data from ref 17. [c]Measured in CH_2Cl_2–MeOH (1:1).

Table 3. Redox Potentials (vs Fc/Fc$^+$) for 2M and 4M[a]

compound	E_{ox}/V	E_{red}/V	ΔE/V[b]
2H$_2$	+0.87	−1.26, −1.83	2.13
2Ni[c]	+0.80	−1.40, −2.02	2.20
2Pd	+0.89	−1.32, −1.92	2.21
2Pt	+0.93	−1.34, −1.82	2.27
4H$_2$	+0.59, +1.00	−1.74, −2.14	2.33
4Ni[c]	+0.59, +1.00	−1.77, −2.20	2.36

[a]Measured in CH_2Cl_2 with Bu_4NPF_6 as supporting electrolyte. [b]Electrochemical HOMO–LUMO gap: $\Delta E = E_{ox,1} - E_{red,1}$. [c]Data from ref 17.

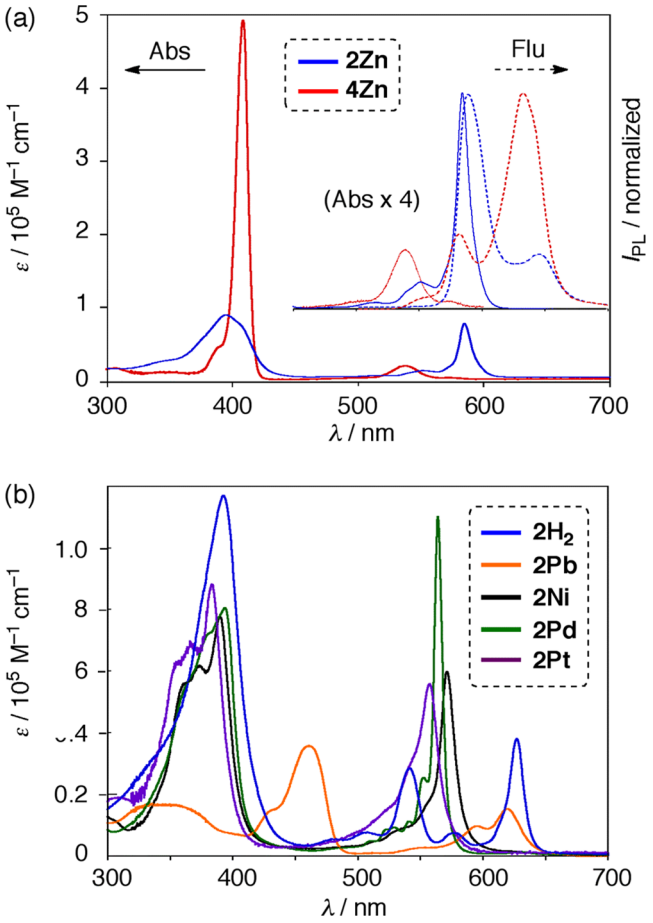

Figure 5. (a) UV–vis absorption (solid line) and fluorescence (dotted line) spectra of **2Zn** (blue) in CH_2Cl_2–MeOH (v/v = 1/1) and **4Zn** (red) in CH_2Cl_2. (b) UV–vis absorption spectra of **2H$_2$** (blue), **2Pb** (orange), **2Ni** (black), **2Pd** (green), and **2Pt** (purple) in CH_2Cl_2.

The absorption and fluorescence spectra of **2Zn**/**4Zn** and **2H$_2$**/**4H$_2$** are shown in Figure 5a and Figure S3 in the Supporting Information, respectively. The longest wavelength Q bands of **2M** (M = H_2, Ni, Zn) are largely intensified and red shifted compared with those of the porphyrin references **4M** (M = H_2, Ni, Zn). In contrast, the Soret bands of **2M** are broadened and blue shifted compared with those of **4M**. The remarkable differences among the extinction coefficients of **2M** and **4M** are consistent with those between **P1** and the 2,3,7,8,12,13,17,18-octaalkylporphyrins reported by Kobayashi and co-workers.[3] The observed results can be rationalized by considering the frontier orbitals of the (diaza)porphyrin π systems and will be discussed in the following section. Figure 5b shows the absorption spectra of the M–DAP derivatives **2M** (M = H_2, Pb, Ni, Pd, Pt). The lead complex **2Pb** displayed relatively weak absorption bands at λ_{max} = 459, 595, and 618 nm in the visible region, which presumably reflects the distorted DAP π plane coordinated to the lead(II) atom. In a series of group 10 metal complexes, the Q bands are blue shifted on going down the periodic table: λ_{max} = 571 nm for **2Ni**, λ_{max} = 564 nm for **2Pd**, and λ_{max} = 557 nm for **2Pt**. This indicates that the S_0–S_1 transition energies increase in the order **2Ni** < **2Pd** < **2Pt**. As shown in Figure 5b, the Q band of each group 10 metal complex looks unsplit, i.e., the splitting of the Q band appears very small. This phenomenon was deeply investigated in ref 3 for the copper complex of **P1** (M = Cu) using magnetic circular dichroism (MCD) spectroscopy; the MCD data clearly showed Faraday B terms corresponding to the Q band at the longest wavelength and another B term of opposite sign at slightly higher energy.

The free base **2H$_2$** and the zinc complex **2Zn** are fluorescent like their porphyrin analogs **4H$_2$** and **4Zn**. When excited at 410 nm, **2H$_2$** and **2Zn** displayed two emission bands at λ_{max} = 631/692 and 588/645 nm, respectively. The optical HOMO–LUMO gaps of **2H$_2$** and **2Zn**, determined from the midpoint of the longest absorption maximum and the shortest emission maximum, are 1.97 and 2.12 eV, respectively. The fluorescence quantum yields of **2H$_2$** (Φ_f = 0.034) and **2Zn** (Φ_f = 0.024) are comparable to those of **4H$_2$** (Φ_f = 0.031) and **4Zn** (Φ_f = 0.031).[27] The fluorescence lifetimes of these free bases and zinc complexes were measured with a streak camera using a femtosecond laser pulse as an excitation source. In all cases, the fluorescence decays obeyed first-order kinetics, and their lifetimes (τ) were determined to be 2.3 ns for **2H$_2$**, 0.53 ns for **2Zn**, 10.4 ns for **4H$_2$**, and 2.3 ns for **4Zn**.[26] From these Φ_f and τ values, the radiation decay rate constants (k_r) and nonradiation decay rate constants (k_{nr}) of the present β-unsubstituted (diaza)porphyrin chromophores were calculated to be $k_r = 1.5 \times 10^7$ s^{-1} and $k_{nr} = 4.2 \times 10^8$ s^{-1} for **2H$_2$**, $k_r = 4.5 \times 10^7$ s^{-1} and $k_{nr} = 1.8 \times 10^9$ s^{-1} for **2Zn**, $k_r = 3.0 \times 10^6$ s^{-1} and $k_{nr} = 9.3 \times 10^7$ s^{-1} for **4H$_2$**, and $k_r = 1.3 \times 10^7$ s^{-1} and $k_{nr} = 4.1 \times 10^8$ s^{-1} for **4Zn**.

dx.doi.org/10.1021/ic301835c | Inorg. Chem. 2012, 51, 12879–12890

5,15-Aza-substitution was found to accelerate both the radiative and the nonradiative decays by ca. 3.5−5 times.

To assess the electrochemical properties of the M−DAPs, the redox potentials of **2M** (M = H_2, Pd, Pt) and **4H$_2$** were measured in CH_2Cl_2 using cyclic voltammetry (CV) and differential pulse voltammetry (DPV) with Bu_4NPF_6 as a supporting electrolyte (Table 3). The voltammograms for the electrochemical oxidation and reduction processes are summarized in Figure S4 in the Supporting Information. In the measurement potential window, all M−DAPs showed one reversible oxidation process and two reversible reduction processes. As reported previously, both the first oxidation potential ($E_{ox,1}$) and the first reduction potential ($E_{red,1}$) of **2Ni** are more positive than the corresponding potentials of **4Ni**.[17] A similar trend was observed for the free bases; **2H$_2$** is easier to reduce but harder to oxidize than **4H$_2$**. Obviously, 5,15-aza-substitution enhances the electron-accepting ability but weakens the electron-donating ability of the β-unsubstituted porphyrin π system. It should be mentioned that the shifts in $E_{red,1}$ values ($\Delta E_{red,1}$ = 0.37−0.48 V, from **4M** to **2M**) are appreciably larger than those in the $E_{ox,1}$ values ($\Delta E_{ox,1}$ = 0.21−0.28 V). This implies that 5,15-aza-substitution has a more significant impact on the LUMO level than on the HOMO level of the porphyrin π system. The observed differences among the optical and electrochemical properties of **2M** and **4M** are in good agreement with those reported for the fully β-substituted analogs (copper complexes and free bases of **P1** and 2,3,7,8,12,13,17,18-octaalkylporphyrin).[3]

Among the group 10 metal complexes, the electron-donating ability decreases in the order **2Ni** ($E_{ox,1}$ = +0.80 V) > **2Pd** ($E_{ox,1}$ = +0.89 V) > **2Pt** ($E_{ox,1}$ = +0.93 V), which agrees well with the trend reported for 5,10,15,20-tetraphenylporphyrin−metal complexes (M−TPP).[28] It is likely that the HOMO levels of these M−DAPs are closely related to the electronegativities of the central metals (vide infra).[23] In contrast, the order of the $E_{red,1}$ values of M−DAP is not straightforward. The electron-accepting ability of M−DAP increases in the order **2Ni** ($E_{red,1}$ −1.40 V) < **2Pt** ($E_{red,1}$ −1.34 V) ≤ **2Pd** ($E_{red,1}$ −1.32 V), although the differences in the potentials are relatively small. The electrochemical HOMO−LUMO gaps (ΔE in Table 3) of these group 10 metal complexes correlate well with their lowest Q-band energies. The combined effects of the meso nitrogen atoms and the central metals on the HOMO and LUMO levels will be discussed in the following section.

To obtain some insight into the optical properties of the electrochemically one-electron-oxidized species from M−DAP, we performed spectroelectrochemical measurements on **2Ni** and **2Pt** in CH_2Cl_2 in the presence of Bu_4NPF_6 (Figure 6). The spectral changes were monitored at several intervals using an optically transparent thin-layer electrochemical cell. Both **2Ni** and **2Pt** displayed clear spectral changes in the one-electron oxidation process to give green solutions; the Soret and Q bands of the neutral species decreased, and characteristic absorption bands of the oxidized species appeared consistently at around 500−700 nm with several isosbestic points. It was reported that the first electrochemical oxidations of Ni−TPP[29] and Pt−TPP[30] under similar conditions generated the corresponding M^{II}−porphyrin π-radical cations, displaying broad absorption bands at around 550−700 nm. By comparison with these results, it can be concluded that the one-electron-oxidized species in the present spectroelectrochemical measurements are M^{II}−DAP π-radical cations (M = Ni, Pt).

Theoretical Studies. To understand the electronic effects of the meso nitrogen atoms and the central metals on the

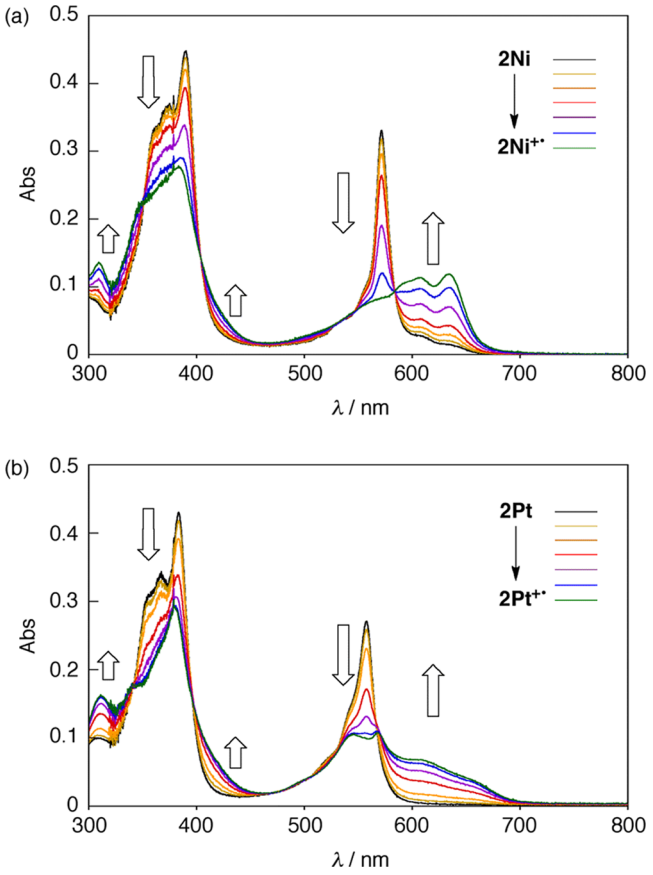

Figure 6. Spectroscopic changes observed for (a) **2Ni** and (b) **2Pt** in the electrochemical oxidation processes from neutral to radical cation species in CH_2Cl_2 containing 0.1 M of Bu_4NPF_6.

frontier orbitals of the β-unsubstituted DAP π systems, DFT calculations on 5,15-diaza-10,20-diphenylporphyrins (**2M-m**) and 5,15-diphenylporphyrins (**4M-m**) were performed using the B3LYP method (M = H_2, Ni, Pd, Pt, Zn; for details, see the Experimental Section). Selected bond lengths and angles for the optimized structures are summarized in Table 4 and Table S3 in the Supporting Information. The bond lengths and angles in the (diaza)porphyrin π planes of **2M-m** (M = H_2, Ni, Pd, Pt) and **4Ni-m** are close to the respective values for **2M** (M = H_2, Ni, Pd, Pt) and **4Ni** obtained by X-ray analyses (Table 1). In the optimized structures, the free bases **2H$_2$-m** and **4H$_2$-m** have C_2 symmetry whereas the metal complexes have D_{2h} symmetry (**2Ni-m**, **4Ni-m**, **4Pt-m**) or D_2 symmetry (**2Pd-m**, **2Pt-m**, **4Pd-m**, **2Zn-m**, **4Zn-m**) including a square-planar metal center. In all of these models, the meso phenyl groups are perpendicular (D_{2h}) or nearly perpendicular (C_2, D_2) to the (diaza)porphyrin π planes.

Harmonic oscillator model of aromaticity (HOMA)[31] values estimated from the C−C/C−N bond lengths of (diaza)porphyrin rings in the models are listed in Table 4. HOMA values (from 1 to 0) have been used as an index for evaluating the degree of geometric aromaticity of cyclic conjugated π systems; values close to 1 represent high aromaticity, whereas those close to 0 represent low aromaticity. The HOMA values with all 28 bonds and with the 18π circuits in the metal complexes **2M-m** are 0.612−0.670 and 0.653−0.741, respectively. As expected, the 18π circuits essentially contribute to the high aromaticity of the entire DAP ring. In each **2M-m** and **4M-m** pair with the same metal center, the HOMA value of **2M-m** is smaller than that of

dx.doi.org/10.1021/ic301835c | Inorg. Chem. 2012, 51, 12879−12890

Table 4. Bond Lengths, Bond Angles, and HOMA Values of 2M-m and 4M-m[a]

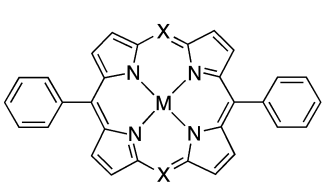

2Ni-m (X = N; M = Ni)
2Pd-m (X = N; M = Pd)
2Pt-m (X = N; M = Pt)
2Zn-m (X = N; M = Zn)
4Ni-m (X = CH; M = Ni)
4Pd-m (X = CH; M = Pd)
4Pt-m (X = CH; M = Pt)
4Zn-m (X = CH; M = Zn)

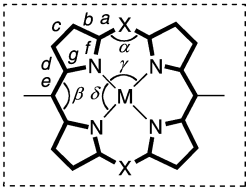

	2Ni-m	2Pd-m	2Pt-m	2Zn-m	4Ni-m	4Pd-m	4Pt-m	4Zn-m
Bond lengths/distances (Å)								
a	1.318	1.324	1.322	1.330	1.378	1.388	1.386	1.394
b	1.442	1.447	1.446	1.449	1.436	1.441	1.439	1.442
c	1.352	1.356	1.356	1.358	1.354	1.358	1.357	1.360
d	1.446	1.453	1.451	1.454	1.441	1.446	1.444	1.448
e	1.391	1.404	1.401	1.410	1.389	1.411	1.396	1.406
f	1.376	1.371	1.376	1.370	1.376	1.364	1.374	1.370
g	1.376	1.369	1.373	1.369	1.380	1.360	1.378	1.373
M−N	1.927	2.006	2.002	2.010	1.968	2.040	2.033	2.048
Bond angles (deg)								
α	121.2	124.1	124.3	124.2	124.1	126.6	126.4	127.1
β	121.8	124.2	124.1	124.5	121.8	124.0	124.1	124.5
γ	89.8	89.9	89.9	89.8	91.0	91.1	91.0	91.2
δ	90.2	90.1	90.1	90.2	89.0	88.9	89.0	88.8
HOMA values								
all[b]	0.670	0.633	0.640	0.618	0.714	0.699	0.704	0.680
18*π*[c]	0.741	0.706	0.714	0.689	0.774	0.751	0.768	0.741

[a]Calculated at the B3LYP level. For basis sets, see Experimental Section. [b]All 28 bonds of the (diaza)porphyrin ring. [c]18*π* circuit.

4M-m, indicating that the geometric aromaticity of M−DAP is somewhat weaker than that of M−porphyrin.

To gain some insight into the ring-current effects of the (diaza)porphyrin *π* systems, we also calculated the nuclear independent chemical shifts (NICS) at two or three positions in the *π* planes as well as the chemical shifts at the *β*-protons of **2M-m** and **4M-m** (M = H_2, Zn) at the same level. As shown in Figure S5 in the Supporting Information, the NICS value at the center of the diazaporphyrin ring in **2H$_2$-m** (−15.88 ppm) is slightly smaller than that of the porphyrin ring in **4H$_2$-m** (−16.04 ppm). The NICS values at the midpoints between the two adjacent pyrrole rings in **2M-m** (−19.19 and −19.67 ppm for **2H$_2$-m**; −18.93 and −19.22 ppm for **2Zn-m**) are also smaller than the respective values in **4M-m** (−19.41 and −19.75 ppm for **4H$_2$-m**; −19.32 ppm for **4Zn-m**). The fact that the NICS values at all positions of **2M-m** are less negative than those of **4M-m** implies that the ring-current effects of **2M-m** are slightly weaker than those of **4M-m**. In both models, the chemical shifts at the *β*-protons neighboring the *meso*-phenyl groups are less deshielded by 0.3−0.5 ppm than those at the other *β*-protons, presumably because of the additional ring-current effects induced by the *meso*-phenyl groups (Figure S5 in the Supporting Information). It should be noted that the chemical shifts calculated at the *β*-protons of **2M-m** (9.57−10.37 ppm for **2H$_2$-m**; 9.85 and 10.27 ppm for **2Zn-m** vs tetramethylsilane) are comparable to or slightly smaller than those of **4M-m** (9.90−10.41 ppm for **4H$_2$-m**; 9.90 and 10.26 ppm for **4Zn-m**). This trend is qualitatively in agreement with the observed ^{1}H NMR chemical shifts of **2M** and **4M** (M = H_2, Zn) in solution. The differences in the HOMA and NICS values between **2M-m** and **4M-m** are, however, very small. In this regard, the aromaticities of the *β*-unsubstituted DAP *π* systems are slightly weaker than those of the porphyrin *π* systems, but they are sufficiently high in terms of both geometric and magnetic criteria.

Selected molecular orbital diagrams of **2M-m** and **4M-m** (M = Ni, Pd, Pt) are shown in Figure 7 together with their orbital energies. As the *meso*-phenyl groups are perpendicular or nearly perpendicular to the (diaza)porphyrin *π* planes, their electronic influences on the 18*π* systems are negligible. The two lowest unoccupied molecular orbitals (LUMO and LUMO+1) and the two highest occupied molecular orbitals (HOMO and HOMO−1) of the porphyrin−metal complexes **4M-m** are almost degenerate. In contrast, the corresponding frontier orbitals of the DAP−metal complexes **2M-m** are definitely nondegenerate. For instance, LUMO and LUMO−1 of **2Ni-m** are split by 0.37 eV, whereas HOMO and HOMO−1 are split by 0.57 eV. Apparently, incorporation of the electronegative nitrogen atoms into the meso positions stabilizes LUMO and HOMO−1 more than LUMO+1 and HOMO, because both LUMO and HOMO−1 have some molecular orbital coefficients at the meso nitrogen atoms. The same is true for the free bases (**2H$_2$-m** vs **4H$_2$-m**) and zinc complexes (**2Zn-m** vs **4Zn-m**) (Figure S6 in Supporting Information). This type of aza-substitution effect is common for the azaporphyrin family and has been interpreted in detail with regard to **P1** derivatives.[3]

The theoretically calculated HOMO and LUMO energy levels of **2M-m** and **4M-m** well explain the fact that the DAP *π* system is harder to oxidize and easier to reduce than the porphyrin *π* system. The differences in the LUMO energies of **2M-m** and **4M-m** (ΔE_{LUMO} = 0.52−0.57 eV) are larger than the differences in the HOMO energies (ΔE_{HOMO} = 0.22−0.38 eV); this is also consistent with the observed differences in the redox potentials ($\Delta E_{red,1}$ = 0.37−0.48 V; $\Delta E_{ox,1}$ = 0.21−0.28 V) of **2M** and **4M** (M = H_2, Ni). The electronic effects of the group 10 metals on the frontier orbitals are worth noting. The HOMO levels deepen in the order **2Ni-m** (−5.61 eV) < **2Pd-m** (−5.72 eV) < **2Pt-m** (−5.76 eV), which matches the order of the $E_{ox,1}$ values of **2Ni** (+0.80 V) < **2Pd** (+0.89 V) < **2Pt** (+0.93 V).

dx.doi.org/10.1021/ic301835c | Inorg. Chem. 2012, 51, 12879−12890

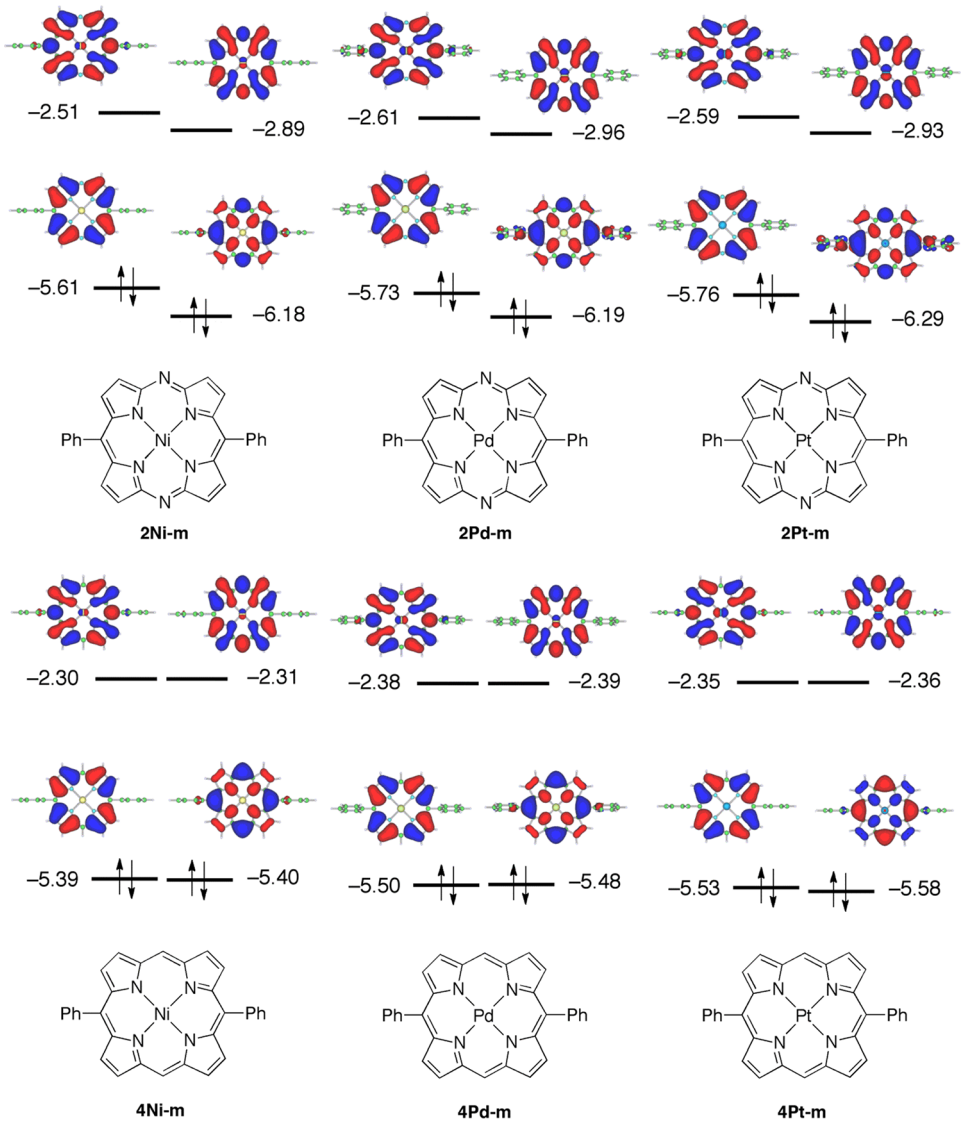

Figure 7. Selected molecular orbitals and their energies (in eV) for **2M-m** (upper) and **4M-m** (lower).

As there is no orbital interaction between the central metal and the DAP ligand in each HOMO, the differences in the orbital energies probably stem from differences in the inductive effects, i.e., the electronegativities of the group 10 metals. The same is true for the HOMO−1 of **2Ni-m** and **2Pd-m** and HOMO−3 of **2Pt-m**, which deepen in the order **2Ni-m** (−6.18 eV) ≤ **2Pd-m** (−6.19 eV) < **2Pt-m** (−6.29 eV). It should be noted that in the group 10 metal complexes two kinds of nearly degenerate ligand-based π orbitals mix with the metal dπ orbitals at relatively high-energy levels. As shown in Figure S6 in the Supporting Information, the resulting dπ-mixed π orbitals of **2Pt-m** (HOMO−1/−2; −6.26/−6.27 eV) are located at much higher energy levels than those of **2Ni-m** (HOMO−2/−3; −6.51/−6.51 eV) and **2Pd-m** (HOMO−2/−3; −6.61/−6.62 eV). This trend clearly reflects the differences in the energy levels of the corresponding dπ orbitals of the divalent group 10 metals;[32] the relatively high-lying dπ orbitals of platinum(II) can interact more strongly with the ligand-based pπ orbitals than can the corresponding orbitals of nickel(II) and palladium(II). A similar dπ−pπ antibonding interaction is also involved in the LUMOs of the group 10 metal complexes. The order of the calculated LUMO levels, **2Ni-m** (−3.08 eV) < **2Pt-m** (−3.13 eV) < **2Pd-m** (−3.18 eV), is in accordance with that of the observed $E_{red,1}$ values, **2Ni** (−1.40 V) < **2Pt** (−1.34 V) < **2Pd** (−1.32 V). Presumably, the LUMO levels are determined by the counterbalancing of two contrary effects, i.e., the inductive effect and the resonance effect (dπ−pπ antiorbital interaction).

The characteristic absorption properties of metalloporphyrins have been theoretically rationalized using Gouterman's four-orbital model; intense Soret bands and weak Q bands are produced by the interactions among the excited configurations (CIs) consisting of four frontier orbitals (accidentally degenerate HOMO/HOMO−1 and degenerate LUMO/LUMO+1).[33] The absorption spectra and electronic structures of the excited states of the M−DAPs were systematically investigated by Kobayashi and co-workers [TD-DFT method; B3LYP/6-31G(d)][3] and Nakatsuji and co-workers (SAC−CI method).[34] To get some insight into the absorption properties of the present β-unsubstituted (diaza)-porphyrin π systems, we calculated the electron-excitation energies of **2M-m** and **4M-m** using the TD-DFT method, and the solvent effects of CH_2Cl_2 were included using a polarizable continuum model (PCM). The excitation energies and their assignments are listed in Table 5. The ratio of the intensities of the Soret and Q bands ($\varepsilon_{Soret}/\varepsilon_Q$) has been used as an index for evaluating the

dx.doi.org/10.1021/ic301835c | Inorg. Chem. 2012, 51, 12879−12890

Table 5. Excitation Energies and Oscillator Strengths of 2M-m and 4M-m Calculated by the TD-DFT Method with Solvent Effects (PCM, CH_2Cl_2)[a]

	excitation energy				
state	(eV)	(nm)	oscillator strength	excitation	weight (%)
2Ni-m					
4	2.41	515	0.273	HOMO → LUMO	86.4
				HOMO−1 → LUMO+1	13.6
5	2.50	496	0.014	HOMO → LUMO+1	57.2
				HOMO−1 → LUMO	42.4
14	3.36	369	0.821	HOMO−1 → LUMO	53.5
				HOMO → LUMO+1	41.1
15	3.44	361	0.545	HOMO−5 → LUMO	38.3
				HOMO−1 → LUMO+1	35.6
16	3.55	349	0.740	HOMO−5 → LUMO	46.9
				HOMO−1 → LUMO+1	44.7
2Pd-m					
1	2.43	509	0.236	HOMO → LUMO	85.2
				HOMO−1 → LUMO+1	14.4
2	2.49	497	0.007	HOMO → LUMO+1	52.1
				HOMO−1 → LUMO	47.4
7	3.26	381	0.660	HOMO−1 → LUMO	47.8
				HOMO → LUMO+1	42.9
9	3.35	370	1.092	HOMO−1 → LUMO+1	70.5
				HOMO → LUMO	12.2
2Pt-m					
3	2.50	497	0.260	HOMO → LUMO	87.2
				HOMO−3 → LUMO+1	12.3
4	2.58	481	0.015	HOMO → LUMO+1	56.6
				HOMO−3 → LUMO	42.8
9	3.32	374	0.618	HOMO−3 → LUMO	51.4
				HOMO → LUMO+1	38.1
10	3.43	362	0.788	HOMO−3 → LUMO+1	59.7
4Ni-m					
4	2.45	506	0.0026	HOMO−1 → LUMO+1	50.8
				HOMO → LUMO	48.7
5	2.45	506	0.0003	HOMO−1 → LUMO	50.3
				HOMO → LUMO+1	49.1
14	3.25	381	1.658	HOMO → LUMO+1	49.0
				HOMO−1 → LUMO	48.8
15	3.27	379	0.932	HOMO → LUMO	49.2
				HOMO−1 → LUMO+1	48.3
4Pd-m					
1	2.47	503	0.0015	HOMO → LUMO+1	50.4
				HOMO−1 → LUMO	49.1
2	2.47	502	0.0006	HOMO → LUMO	51.6
				HOMO−1 → LUMO+1	47.8
6	3.23	384	1.634	HOMO−1 → LUMO+1	50.9
				HOMO → LUMO	46.4
7	3.25	382	0.871	HOMO−1 → LUMO	49.8
				HOMO → LUMO+1	47.4
4Pt-m					
1	2.55	487	0.005	HOMO → LUMO+1	53.1
				HOMO−1 → LUMO	46.4
2	2.55	486	0.001	HOMO → LUMO	52.6
				HOMO−1 → LUMO+1	46.8
9	3.29	376	1.611	HOMO−1 → LUMO+1	50.8
				HOMO → LUMO	46.1
10	3.31	374	0.851	HOMO−1 → LUMO	50.8
				HOMO → LUMO+1	45.5

[a]The states whose oscillator strengths are less than 0.2 are not included except for Q bands.

degree of CI: the larger the ratio, the stronger the CI. The nickel porphyrin **4Ni-m** possesses nearly degenerate HOMO/HOMO−1 and LUMO/LUMO+1, which produces a strong CI for $\pi-\pi^*$ transitions. Indeed, the theoretically predicted Q band (507 nm, 2.45 eV) has a very small oscillator strength (f = 0.003), which explains the relatively large ratio of the extinction coefficients observed for **4Ni** ($\varepsilon_{Soret}/\varepsilon_Q$ = 26). In sharp contrast, **2Ni-m** involves nondegenerate HOMOs and LUMOs, and this results in weak CI. This is reflected in the large oscillator strength (f = 0.284) for the Q band of **2Ni-m** (515 nm, 2.40 eV) and the small $\varepsilon_{Soret}/\varepsilon_Q$ ratio (1.6) of **2Ni**. The red-shifted appearance of the Q band for **2Ni-m** (vs **4Ni-m**), i.e., a decrease in the excitation energy of the Q band, is attributed to the large weight of the HOMO-to-LUMO transition (86.4%). TD-DFT calculations for the other **2M-m** and **4M-m** models gave similar results: (i) the oscillator strengths of the Q bands of **2M-m** are considerably larger than those of **4M-m**, (ii) the Q bands of **2M-m** are red shifted compared with those of **4M-m**, and (iii) the Soret bands of **2M-m** are split and blue shifted compared with those of **4M-m**. TD-DFT calculations of the group 10 metal complexes also revealed that the lowest transition energies of their DAP π systems increase in the order **2Ni-m** < **2Pd-m** < **2Pt-m**, which correlates well with the observed order of **2Ni** < **2Pd** < **2Pt** (vide supra). It is now evident that the 5,15-aza-substitution had a significant impact on the intrinsic absorption properties of the β-unsubstituted porphyrin π systems.

CONCLUSION

New examples of the β-unsubstituted 5,15-diaza-10,20-dimesitylporphyrins, namely, free base and lead(II), palladium(II), platinum(II), and zinc(II) complexes, were prepared from mesityl-substituted bis(5,5′-dibromodipyrrin). In addition, the coordination spheres, optical and electrochemical properties, and aromaticities of a series of M−DAPs were comprehensively investigated using X-ray crystallography, absorption/emission spectroscopy, NMR spectroscopy, CV/DPV, and theoretical calculations. Incorporation of two nitrogen atoms into the meso positions of the β-unsubstituted porphyrin skeleton was found to (i) contract the N_4 coordination sphere, (ii) significantly increase the intensity of the Q band and narrow the HOMO−LUMO gap, (iii) greatly enhance the electron-accepting ability but weaken the electron-donating ability, (iv) accelerate the radiative decay rate from the S_1 state, and (v) slightly reduce the aromaticity of the π system. The central metals of the group 10 metal complexes also make small but distinct impacts on the fundamental properties of the DAP π systems, as a result of the inductive and resonance effects. The fundamental information obtained in this study will be helpful for the rational design of new classes of diazaporphyrin-based materials for uses in optoelectronics and as metal catalysts.

EXPERIMENTAL SECTION

General Remarks. All melting points were recorded on a Yanagimoto micromelting point apparatus and are uncorrected. ^1H and $^{13}C\{^1H\}$

dx.doi.org/10.1021/ic301835c | Inorg. Chem. 2012, 51, 12879−12890

NMR spectra were recorded on a JEOL JNM-EX400 or JEOL JNM-AL300 spectrometer using CD_2Cl_2 as a solvent unless otherwise noted. Chemical shifts are reported in ppm as relative values vs tetramethylsilane (internal reference). Matrix-assisted laser desorption/ionization (MALDI) time-of-flight mass spectra (TOF) were measured on a SHIMADZU Biotech AXIMA-CFR spectrometer. High-resolution mass spectra (HRMS) were obtained on a Thermo EXACTIVE spectrometer. UV−vis absorption spectra were measured on a PerkinElmer Lambda 900 UV/vis/NIR spectrometer. Steady-state fluorescence spectra were recorded with a HORIBA SPEX Fluoromax-3 spectrofluorometer. Absolute fluorescence quantum yields were determined by a Hamamatsu Photonics Quantaurus-QY spectrometer. Electrochemical measurements were performed on a CH Instruments model 660A electrochemical workstation using a glassy carbon working electrode, a platinum wire counter electrode, and an Ag/Ag^+ [0.01 M $AgNO_3$, 0.1 M Bu_4NPF_6 (MeCN)] reference electrode. Potentials were calibrated with ferrocene/ferrocenium [E_{mid} = +0.20 V vs $Ag/AgNO_3$]. Compounds **3**,[17] **4H$_2$**,[25] and **4Zn**[25] were prepared according to reported procedures. Sodium azide (>98%) and dehydrated DMF (water content <0.005%) were purchased from Wako Pure Chemical Industries. All reactions were performed under an argon atmosphere.

Synthesis of 1Zn. A mixture of **3** (300 mg, 0.714 mmol), $Zn(OAc)_2$ (79 mg, 0.43 mmol), and MeOH (180 mL) was stirred at room temperature. After 3 h, the deposited orange solid was filtered off, washed with MeOH, and dried to give **1Zn** (267 mg, 83%). ^{1}H NMR (400 MHz, CD_2Cl_2): δ 2.11 (s, 12H, *o*-Me), 2.37 (s, 6H, *p*-Me), 6.47 (d, J = 4.4 Hz, 4H, pyrrole-β), 6.47 (d, J = 4.4 Hz, 4H, pyrrole-β), 6.96 (s, 4H, Ar-*m*). HR-MS (ESI) calcd for $C_{36}H_{31}Br_4N_4Zn$: 902.8527. Found: m/z 902.8498 ($[M + H]^+$)

Synthesis of 2Pb and 2H$_2$. A mixture of **3** (607 mg, 1.44 mmol), $Pb(acac)_2$ (324 mg, 0.799 mmol), sodium azide (207 mg, 3.18 mmol), and MeOH (300 mL) was heated at reflux. The progress of the reaction was monitored by TLC. After 48 h, toluene and water were added to the reaction mixture, and the organic phase was separated, washed with water, dried over Na_2SO_4, and evaporated under reduced pressure to leave a solid residue, which was then subjected on silica-gel column chromatography (hexane/EtOAc = 5/2). Compounds **2H$_2$** (trace) and **2Pb** (49 mg, 9%) were isolated as purple solids. When DMF was used as the solvent, the reaction was complete after several hours at 110 °C to produce both **2H$_2$** and **2Pb**. However, the isolated yields of **2H$_2$** and **2Pb** varied widely and irregularly (from trace to 33%) depending on the reaction conditions employed. **2Pb**: Mp >300 °C. ^{1}H NMR (300 MHz, CD_2Cl_2): δ 1.50 (s, 6H, *p*-Me), 2.04 (s, 6H, *o*-Me), 2.56 (s, 6H, *o*-Me), 7.23 (s, 2H, Ar-*m*), 7.30 (s, 2H, Ar−*m*), 8.83 (d, J = 4.8 Hz, 4H, pyrrole-β), 9.19 (d, J = 4.8 Hz, 4H, pyrrole-β). ^{13}C{^{1}H} NMR (100 MHz, CD_2Cl_2): δ 157.9, 150.8, 140.2, 139.2, 138.8, 134.0, 133.9, 128.4, 128.2, 123.8, 22.5, 21.6. HR-MS (ESI) calcd for $C_{36}H_{31}N_6Pb$: 753.2355. Found: m/z 753.2329 ($[M + H]^+$). UV−vis (CH_2Cl_2): λ_{max} (ε) 334 (16 000), 459 (35 000), 595 (9600), 618 nm (15 000 M^{-1} cm^{-1}). **2H$_2$**: Mp >300 °C. ^{1}H NMR (400 MHz, CD_2Cl_2): δ −2.61 (s, 2H, NH), 1.83 (s, 12H, *p*-Me), 2.64 (s, 6H, *o*-Me), 7.33 (s, 4H, Ar-*m*), 8.84 (d, J = 4.8 Hz, 4H, pyrrole-β), 9.24 (d, J = 4.8 Hz, 4H, pyrrole-β). ^{13}C{^{1}H} NMR (100 MHz, CD_2Cl_2): δ 151.0, 144.5, 139.3, 139.0, 135.5, 134.5, 133.8, 128.3, 121.2, 30.1, 21.5. HR-MS (ESI) calcd for $C_{36}H_{32}N_6$: 547.2956. Found: m/z 547.2854 ($[M]^+$). UV−vis (CH_2Cl_2): λ_{max} (ε) 393 (130 000), 541 (32 000), 627 nm (42 000 $M^{-1}cm^{-1}$).

Synthesis of 2H$_2$ from 2Pb. To a solution of **2Pb** (30 mg, 0.040 mmol) in CH_2Cl_2 (30 mL) was added trifluoroacetic acid (2 mL, 27 mmol), and the resulting mixture was stirred at room temperature. After 1h, the mixture was washed with an aqueous $NaHCO_3$ solution and brine, dried over Na_2SO_4, and evaporated under reduced pressure to leave a solid residue, which was then recrystallized from CH_2Cl_2−MeOH to give **2H$_2$** as a purple solid (21 mg, 95%).

Synthesis of 2Pd. A solution of **2H$_2$** (11.2 mg, 0.0204 mmol) in $CHCl_3$ (10 mL) was treated with a solution of $Pd(OAc)_2$ (12.4 mg, 0.0552 mmol) in methanol (2 mL) at 70 °C. After 26 h, water was added and the aqueous layer was extracted with CH_2Cl_2. The combined organic extracts were washed with a saturated aqueous $NaHCO_3$ solution and brine, dried over Na_2SO_4, and evaporated under reduced pressure to leave a solid residue, which was then subjected to silica gel column chromatography (hexane/EtOAc = 5/1) followed by reprecipitation from CH_2Cl_2−MeOH. Compound **2Pd** was isolated as a purple solid (R_f = 0.4; 11.8 mg, 89%). Mp > 300 °C. ^{1}H NMR (400 MHz, CD_2Cl_2): δ 1.82 (s, 12H, *o*-Me), 2.63 (s, 6H, *p*-Me), 7.33 (s, 4H, Ar-*m*), 8.78 (d, J = 4.8 Hz, 4H, pyrrole-β), 9.15 (d, J = 4.8 Hz, 4H, pyrrole-β). ^{13}C{^{1}H} NMR (CD_2Cl_2): δ 148.0, 142.0, 140.0, 139.1, 135.7, 133.3, 128.4, 21.8, 21.6. HR-MS (ESI) calcd for $C_{36}H_{31}N_6Pd$: 653.1645. Found: m/z 653.1639 ($[M + H]^+$). UV−vis (CH_2Cl_2): λ_{max} (ε) 394 (80 500), 564 nm (110 000 M^{-1} cm^{-1}).

Synthesis of 2Pt. $PtCl_2$ (61.2 mg, 0.230 mmol) was heated at reflux in benzonitrile (60 mL) for 1 h. To the resulting solution was added **2H$_2$** (12.5 mg, 0.0228 mmol), and the reaction mixture was refluxed for further 2 days. Benzonitrile (60 mL) was removed under reduced pressure, and the crude product was purified by column chromatography on silica gel (hexane/EtOAc = 5/1). Reprecipitation of the eluted solid from CH_2Cl_2−MeOH afforded **2Pt** as a purple solid (R_f = 0.55; 9.2 mg, 54%). Mp > 300 °C. ^{1}H NMR (400 MHz, CD_2Cl_2): δ 1.82 (s, 12H, *o*-Me), 2.63 (s, 6H, *p*-Me), 7.31 (s, 4H, Ar-*m*), 8.70 (dd, J = 5.4, 11.2 Hz, 4H, pyrrole-β), 9.08 (dd, J = 5.4, 11.2 Hz, 4H, pyrrole-β). HR-MS (ESI) calcd for $C_{36}H_{31}N_6Pt$: 741.2231. Found: m/z 741.2209 ($[M + H]^+$). UV−vis (CH_2Cl_2): λ_{max} (ε) 383 (88 100), 557 nm (55 900 M^{-1} cm^{-1}).

Synthesis of 2Zn. A mixture of **2H$_2$** (50 mg, 0.091 mmol) and $Zn(OAc)_2$ (82 mg, 0.45 mmol) was stirred vigorously in $CHCl_3$−methanol (15 mL/1 mL) at 70 °C. After 24 h, water was added and the aqueous layer was extracted with CH_2Cl_2. The combined organic extracts were washed with a saturated aqueous $NaHCO_3$ solution and brine, dried over Na_2SO_4, and evaporated under reduced pressure to leave a solid residue, which was then subjected to silica gel column chromatography ($CHCl_3$). Compound **2Zn** was isolated as a purple solid (51 mg, 92%) by reprecipitation from CH_2Cl_2−MeOH. Mp > 300 °C. ^{1}H NMR (300 MHz, CD_2Cl_2−CD_3OD, 1:1): δ 1.79 (s, 12H, *o*-Me), 2.60 (s, 6H, *p*-Me), 7.29 (s, 4H, Ar-*m*), 8.78 (d, J = 4.8 Hz, 4H, pyrrole-β), 9.15 (d, J = 4.8 Hz, 4H, pyrrole-β). ^{13}C{^{1}H} NMR (300 MHz, CD_2Cl_2−CD_3OD, 1:1): δ 151.0, 144.5, 139.3, 139.0, 135.5, 134.5, 133.8, 128.3, 121.2, 30.1, 21.5. HR-MS (ESI) calcd for $C_{36}H_{30}N_6Zn$: 610.18179. Found: m/z 610.18447 ($[M]^+$). UV−vis (CH_2Cl_2−MeOH; 1:1): λ_{max} (ε) 394 (83 300), 552 (8900), 584 nm (71 900 M^{-1} cm^{-1}).

Spectral Data for 4H$_2$. ^{1}H NMR (400 MHz, CD_2Cl_2): δ −3.12 (s, 2H, NH), 1.83 (s, 12H, *o*-Me), 2.65 (s, 6H, *p*-Me), 7.34 (s, 4H, Ar-*m*), 8.85 (d, J = 4.4 Hz, 4H, pyrrole-β), 9.36 (d, J = 4.4 Hz, 4H, pyrrole-β), 10.24 (s, 2H, *meso*). UV−vis (CH_2Cl_2): λ_{max} (ε) 403 (320 000), 500 (20 000), 534 (4000), 572 (7900), 627 (1600 M^{-1} cm^{-1}).

Spectral Data for 4Zn. ^{1}H NMR (300 MHz, CD_2Cl_2): δ 1.81 (s, 12H, *o*-Me), 2.66 (s, 6H, *p*-Me), 7.34 (s, 4H, Ar-*m*), 8.93 (d, J = 4.8 Hz, 4H, pyrrole-β), 9.41 (d, J = 4.8 Hz, 4H, pyrrole-β), 10.26 (s, 2H, *meso*). UV−vis (CH_2Cl_2): λ_{max} (ε) 409 (490 000), 538 (15 600), 573 nm (2200 M^{-1} cm^{-1}).

X-ray Crystallographic Analysis. Single crystals of **1Zn**, **2H$_2$**, **2Pd**, **2Pt**, and **4Ni** were grown from CH_2Cl_2−MeOH. All measurements were made on a Rigaku Saturn CCD area detector with graphite-monochromated Mo Kα radiation (0.71070 Å) at −130 °C. Data were corrected for Lorentz and polarization effects. Structures were solved using direct methods[35] and refined by full-matrix least-squares techniques against F^2 using SHELXL-97.[36] Non-hydrogen atoms were refined anisotropically, and hydrogen atoms were refined using the rigid model. **1Zn**: $C_{36}H_{30}Br_4N_4Zn$, MW = 903.65, 0.20 × 0.15 × 0.05 mm, monoclinic, $P2_1/n$, a = 11.116(5) Å, b = 11.382(5) Å, c = 27.793(13) Å, β = 94.543(8)°, V = 3505(3) Å^3, Z = 4, ρ_{calcd} = 1.712 g cm^{-3}, μ = 52.91 cm^{-1}, collected 25 541, independent 7841, parameters 406, R_w = 0.1932, R = 0.0656 ($I > 2.0\sigma(I)$), GOF = 1.100. **2H$_2$**: $C_{36}H_{32}N_6$, MW = 548.68, 0.55 × 0.30 × 0.10 mm, monoclinic, $P2_1/c$, a = 8.412(4) Å, b = 23.757(10) Å, c = 7.831(4) Å, β = 113.799(5)°, V = 1431.9(11) Å^3, Z = 2, ρ_{calcd} = 1.273 g cm^{-3}, μ = 0.77 cm^{-1}, collected 12 409, independent 3094, parameters 190, R_w = 0.1483, R = 0.0728 ($I > 2.0\sigma(I)$), GOF = 1.173. **2Pd**: $C_{36}H_{30}N_6Pd$, MW = 653.06, 0.35 × 0.30 × 0.02 mm, trigonal, $P-3$, a = b = 15.384(5) Å, c = 11.304(4) Å, γ = 120°, V = 2317.1(12) Å^3, Z = 3, ρ_{calcd} = 1.404 g cm^{-3}, μ = 6.36 cm^{-1}, collected 18 116, independent 3520, parameters 196, R_w = 0.0876, R = 0.0488 ($I > 2.0\sigma(I)$), GOF = 1.017. **2Pt**: $C_{36}H_{30}N_6Pt$, MW = 741.75, 0.30 × 0.20 ×

0.02 mm, trigonal, $P\bar{3}$, $a = b = 15.3958$ (18) Å, $c = 11.2532(13)$ Å, $\gamma = 120°$, $V = 2310.0(5)$ Å^3, $Z = 3$, $\rho_{calcd} = 1.600$ g cm^{-3}, $\mu = 45.91$ cm^{-1}, collected 27 782, independent 3536, parameters 196, $R_w = 0.0533$, $R = 0.0235$ ($I > 2.0\sigma(I)$), GOF = 1.056. **4Ni**: $C_{38}H_{32}N_4Ni$, MW = 603.39, 0.35 × 0.15 × 0.04 mm, monoclinic, $P2_1/c$, $a = 13.345(3)$ Å, $b = 13.790(3)$ Å, $c = 8.1213(16)$ Å, $\beta = 101.114(2)°$, $V = 1466.6(5)$ Å^3, $Z = 2$, $\rho_{calcd} = 1.366$ g cm^{-3}, $\mu = 6.96$ cm^{-1}, collected 11 220, independent 3242, parameters 196, $R_w = 0.1014$, $R = 0.0390$ ($I > 2.0\sigma(I)$), GOF = 1.108.

Fluorescence Lifetime Measurements. Fluorescence lifetimes of **2H$_2$**, **2Zn**, **4H$_2$**, and **4Zn** were measured in CH_2Cl_2 (**2H$_2$**, **4H$_2$**, **4Zn**) or CH_2Cl_2–MeOH (**2Zn**) using a streak camera as a fluorescence detector. All samples were excited by the second harmonic output (400 nm) from the amplified Ti:Sapphire laser system.

Computational Details. Geometries of all models were optimized by the DFT method. The basis sets used were the 6-311G(d,p) basis set[37] for H, C, and N, the Wachters–Hay all-electron basis set[38] supplemented with one f-function for Ni and Zn [f exponents 1.29 (Ni) and 1.62 (Zn)], and the Los Alamos triple-ζ basis sets supplemented with one f-function [f exponents 1.472 (Pd) and 0.993 (Pt)] with associated pseudopotentials (LANL2TZ(f)).[39] The functional of DFT was the Becke, three-parameter, Lee–Yang–Parr (B3LYP) exchange-correlation functional.[40] We confirmed that the optimized geometries were not in saddle but in stable points. Cartesian coordinates are summarized in Tables S1 and S2 in the Supporting Information. The nucleus-independent chemical shift (NICS) values[41] and proton chemical shifts (vs tetramethylsilane) were calculated at the Hartree–Fock level with gauge-including atomic orbitals (GIAOs) at the DFT-optimized structures. The basis set used in the NICS value and chemical shift calculations was 6-31+G(d).[42] Excitation energies and oscillator strengths were computed with the time-dependent density functional theory (TD-DFT) method, in which the solvent effect of CH_2Cl_2 was included by the PCM method.[43] All calculations were carried out using the Gaussian 09 suite of programs.[44]

Spectroelectrochemical Measurements. Spectroelectrochemical measurements were carried out with a custom-made optically transparent thin-layer electrochemical cell (light pass length = 1 mm) equipped with a platinum mesh, a platinum coil, and a silver wire as the working, counter, and pseudoreference electrodes, respectively. Absorption spectra were measured with a Perkin-Elmer Lambda 900 UV/vis/NIR spectrometer, and the potential was applied with an ALS/chi electrochemical analyzer model 612A.

■ ASSOCIATED CONTENT

Ⓢ Supporting Information

Complete ref 44, spectral and theoretical data, ^{1}H NMR charts for some compounds, and CIF files. This material is available free of charge via the Internet at http://pubs.acs.org.

■ AUTHOR INFORMATION

Corresponding Author

*E-mail: matano@scl.kyoto-u.ac.jp.

Notes

The authors declare no competing financial interest.

■ ACKNOWLEDGMENTS

This work was partially supported by a Grant-in-Aid for Scientific Research on Innovative Areas (No. 23108708, π-Space) from MEXT, Japan. We thank Mr. Daisuke Sakamaki (Kyoto University) for his help in the spectroelectrochemical measurements. Y.M. deeply acknowledges Prof. Shigeki Kawabata (Toyama Prefectural University) for his valuable suggestions concerning the synthesis of M–DAPs.

■ REFERENCES

(1) Fischer, H.; Harberland, H.; Müller, A. *Justus Liebigs Ann. Chem* **1936**, *521*, 122–128.

(2) Kobayashi, N. In *The Porphyrin Handbook*; Kadish, K. M., Smith, R. M., Guilard, R., Eds.; Academic Press: San Diego, 2000; Vol. *2*, pp 301–360.

(3) Ogata, H.; Fukuda, T.; Nakai, K.; Fujimura, Y.; Neya, S.; Stuzhin, P. A.; Kobayashi, N. *Eur. J. Inorg. Chem.* **2004**, 1621–1629.

(4) Stuzhin and Khelevina summarized the metal complex formation of diazaporphyrins, see: Stuzhin, P. A.; Khelevina, O. G. *Coord. Chem. Rev.* **1996**, *147*, 41–86.

(5) (a) Kaczmarzyk, T.; Jackowski, T.; Dzilinski, K.; Kania, L. *Acta Phys. Pol., A* **2009**, *115*, 656–659. (b) Stuzhin, P. A.; Nefedov, S. E.; Kumeev, R. S.; Ul-Haq, A.; Minin, V. V.; Ivanova, S. S. *Inorg. Chem.* **2010**, *49*, 4802–4813. (c) Stuzhin, P. A.; Ul-Haq, A.; Nefedov, S. E.; Kumeev, R. S.; Koifman, O. I. *Eur. J. Inorg. Chem.* **2011**, 2567–2578.

(6) Neya, S.; Hori, H.; Imai, K.; Kawamura-Konishi, Y.; Suzuki, H.; Shiro, Y.; Iizuka, T.; Funasaki, N. *J. Biochem.* **1997**, *121*, 654–660.

(7) Ohgo, Y.; Neya, S.; Uekusa, H.; Nakamura, M. *Chem. Commun.* **2006**, 4590–4592 (Correction: **2008**, 6609).

(8) Shinmori, H.; Kodaira, F.; Matsugo, S.; Kawabata, S.; Osuka, A. *Chem. Lett.* **2005**, *34*, 322–323.

(9) Optical oxygen-sensing with palladium and platinum complexes of 5,10-diazaporphyrin was also reported. Borisov, S. M.; Zenkl, G.; Klimant, I. *ACS Appl. Mater. Interfaces* **2010**, *2*, 366–374.

(10) Okujima, T.; Jin, G.; Otsubo, S.; Aramaki, S.; Ono, N.; Yamada, H.; Uno, H. *J. Porphyrins Phthalocyanines* **2011**, *15*, 697–703.

(11) Pan, N.; Bian, Y.; Fukuda, T.; Yokoyama, M.; Li, R.; Neya, S.; Jiang, J.; Kobayashi, N. *Inorg. Chem.* **2004**, *43*, 8242–8244.

(12) Pan, N.; Bian, Y.; Yokoyama, M.; Li, R.; Fukuda, T.; Neya, S.; Jiang, J.; Kobayashi, N. *Eur. J. Inorg. Chem.* **2008**, 5519–5523.

(13) Chizhova, N. V.; Toldina, O. V.; Mamardashvili, N. Z. *Russ. J. Inorg. Chem. (Engl. Transl.)* **2008**, *53*, 1401–1404.

(14) Harris, R. L. N.; Johnson, A. W.; Kay, I. T. *J. Chem. Soc. (C)* **1966**, 22–29.

(15) (a) Galanin, N. E.; Kudrik, E. V.; Shaposhnikov, G. P. *Russ. J. Gen. Chem.* **2005**, *75*, 651–655. (b) Galanin, N. E.; Yakubov, L. A.; Kudrik, E. V.; Shaposhnikov, G. P. *Russ. J. Gen. Chem.* **2008**, *78*, 1436–1440. (c) Bykova, V.; Usol'tseva, N.; Kudrik, E.; Galanin, N.; Shaposhnikov, G.; Yakubov, L. *Mol. Cryst. Liq. Cryst.* **2008**, *494*, 38–47.

(16) Two β-unsubstituted DAP–copper complexes were reported in a patent, although the yields and the spectral data are not described. Ogiso, A.; Inoue, S.; Nishimoto, T.; Tsukahara, H.; Misawa, T.; Koike, T.; Mihara, N.; Murayama, S.; Nara, R. WO-A1-2001047719, 2001.

(17) Matano, Y.; Shibano, T.; Nakano, H.; Imahori, H. *Chem.—Eur. J.* **2012**, *18*, 6208–6216.

(18) Shinokubo and coworkers independently reported the formation of **2Ni** in their original synthesis of azacorroles. See: Horie, M.; Hayashi, Y.; Yamaguchi, S.; Shinokubo, H. *Chem.—Eur. J.* **2012**, *18*, 5919–5923.

(19) Maeda, H.; Hashimoto, T.; Fujii, R.; Hasegawa, M. *J. Nanosci. Nanotechnol.* **2009**, *9*, 240–248.

(20) 3,7,13,17-Tetramethyl-2,8,12,18-tetrabutyl-5,15-diazaporphyrin free base was prepared from the corresponding dibromodipyrrin hydrobromide, NaN_3, and $Pb(acac)_2$ in DMF. See: Khelevina, O. G.; Chizhova, N. V.; Stuzhin, P. A.; Semeikin, A. S.; Berezin, B. D. *Russ. J. Phys. Chem. (Engl. Transl.)* **1997**, *71*, 74–78.

(21) All attempts to cleave the M–N bonds (M = Ni, Cu) of **2Ni** and **2Cu** with protic acids (trifluoroacetic acid, sulfuric acid, and a mixture of trifluoroacetic acid and sulfuric acid) have resulted in failure.

(22) When the same reaction was conducted in DMF at 110 °C, a mixture of **2Pb** and **2H$_2$** was obtained; however, the reproducibility of their yields was not satisfactory.

(23) Emsley, J. *The Elements*, 3rd ed.; Oxford University Press: New York, 1998. Covalent bond radii and electronegativities (Pauling): 1.54 Å and 2.33 for Pb; 1.15 Å and 1.91 for Ni; 1.28 Å and 2.20 for Pd; and 1.29 Å and 2.28 for Pt; 1.25 Å and 1.65 for Zn; 1.50 Å and 1.78 for In.

(24) (a) Stuzhin, P. A.; Goeldner, M.; Homborg, H.; Semeikin, A. S.; Migalova, I. S.; Wolowiec, S. *Mendeleev Commun. (Engl. Transl.)* **1999**, *9*, 134–136. (b) Khelevina, O. G.; Stuzhin, P. A.; Migalova, I. S.; Shukhto, O. V. *Russ. J. Gen. Chem. (Engl. Transl.)* **2001**, *71*, 1647–

1652. (c) Stuzhin, P. A.; Ivanova, S. S.; Migalova, I. S. *Russ. J. Gen. Chem. (Engl. Transl.)* **2004**, *74*, 1435−1445.
(25) Yu, L.; Muthukumaran, K.; Sazanovich, I. V.; Kirmaier, C.; Hindin, E.; Diers, J. R.; Boyle, P. D.; Bocian, D. F.; Holten, D.; Lindsey, J. S. *Inorg. Chem.* **2003**, *42*, 6629−6647.
(26) We have not succeeded in obtaining good-quality X-ray diffraction data for **2Pb**. However, preliminary X-ray analysis of **2Pb** showed that its lead center deviates greatly from the diazaporphyrin 24-atom mean π plane, as deduced from ^{1}H NMR observations.
(27) Lindsey, Bocian, Holton, and co-workers reported the optical data for $\mathbf{4H_2}$ and **4Zn**, where the Φ_f and τ values of **4Zn** in toluene were reported to be 0.024 and 2.6 ns, respectively. See ref 25.
(28) Takeda, J.; Sato, M. *Chem. Lett.* **1995**, 939−940 . $E_{ox,1}$ and $E_{red,1}$ values are referenced to the Fc/Fc^+ couple (+0.38 V vs. SCE): +0.66 and −1.64 V for Ni−TPP; +0.82 and −1.62 V for Pd−TPP; +0.92 and −1.59 V for Pt−TPP. These values are based on the reported $E_{ox,1}$ and $E_{red,1}$ values vs SCE (in CH_2Cl_2 with Bu_4NPF_6 as an electrolyte).
(29) (a) Dolphin, D.; Niem, T.; Felton, R. H.; Fujita, I. *J. Am. Chem. Soc.* **1975**, *97*, 5288−5290. (b) Johnson, E. C.; Niem, T.; Dolphin, D. *Can. J. Chem.* **1978**, *56*, 1381−1388. (c) Chang, D.; Malinski, T.; Ulman, A.; Kadish, K. M. *Inorg. Chem.* **1984**, *23*, 817−824.
(30) (a) Ou, Z.; Cheng, P.; Kadish, K. M. *Dalton Trans.* **2010**, *39*, 11272−11276. (b) Cheng, P.; Finikova, O. S.; Ou, Z.; Vinogradov, S. A.; Kadish, K. M. *Inorg. Chem.* **2012**, *51*, 6200−6210.
(31) (a) Kruszewski, J.; Krygowski, T. M. *Tetrahedron Lett.* **1972**, 3839−3842. (b) Krygowski, T. M. *J. Chem. Inf. Comput. Sci.* **1993**, *33*, 70−78. (c) Krygowski, T. M.; Ciesielski, A.; Bird, C. W.; Kotschy, A. *J. Chem. Inf. Comput. Sci.* **1995**, *35*, 203−210. (d) Cyrañski, M. K.; Krygowski, T. M.; Wisiorowski, M.; van Eikema Hommes, N. J. R.; Schleyer, P.; von, R. *Angew. Chem., Int. Ed.* **1998**, *37*, 177−180.
(32) For example, see: Matano, Y.; Matsumoto, K.; Hayashi, H.; Nakao, Y.; Kumpulainen, T.; Chukharev, V.; Tkachenko, N. V.; Lemmetyinen, H.; Shimizu, S.; Kobayashi, N.; Sakamaki, D.; Ito, A.; Tanaka, K.; Imahori, H. *J. Am. Chem. Soc.* **2012**, *134*, 1825−1839.
(33) (a) Seybold, P. G.; Gouterman, M. *J. Mol. Spectrosc.* **1969**, *31*, 1−13. (b) Bajema, L.; Gouterman, M.; Rose, C. B. *J. Mol. Spectrosc.* **1971**, *39*, 421−431.
(34) Hasegawa, J.; Kimura, T.; Nakatsuji, H. *J. Porphyrins Phthalocyanines* **2005**, *9*, 305−315 . SAC-CI: Symmetry Adapted Cluster Configuration Interaction.
(35) (a) SIR92 (for **1Zn**, **4Ni**): Altomare, A.; Cascarano, G.; Giacovazzo, C.; Guagliardi, A.; Burla, M.; Polidori, G.; Camalli, M. *J. Appl. Crystallogr.* **1994**, *27*, 435−436. (b) SIR2008 (for $\mathbf{2H_2}$, **2Pd**, **2Pt**): Burla, M. C.; Caliandro, R.; Camalli, M.; Carrozzini, B.; Cascarano, G. L.; De Caro, L.; Giacovazzo, C.; Polidori, G.; Siliqi, D.; Spagna, R. *J. Appl. Crystallogr.* **2007**, *40*, 609−613.
(36) SHELXL-97: Sheldrick, G. M. *Acta Crystallogr.* **2008**, *A64*, 112−122.
(37) Krishnan, R.; Binkley, J. S.; Seeger, R.; Pople, J. A. *J. Chem. Phys.* **1980**, *72*, 650−654.
(38) (a) Wachters, A. J. H. *J. Chem. Phys.* **1970**, *52*, 1033−1036. (b) Hay, P. J. *J. Chem. Phys.* **1977**, *66*, 4377−4384. (c) Raghavachari, K.; Trucks, G. W. *J. Chem. Phys.* **1989**, *91*, 1062−1065.
(39) Hay, P. J.; Wadt, W. R. *J. Chem. Phys.* **1985**, *82*, 299−310.
(40) Becke, A. D. *J. Chem. Phys.* **1993**, *98*, 5648−5652.
(41) Schleyer, P. v. R.; Maerker, C.; Dransfeld, A.; Jiao, H.; van Eikema Hommes, N. J. R. *J. Am. Chem. Soc.* **1996**, *118*, 6317−6318.
(42) (a) Hehre, W. J.; Ditchfield, R.; Pople, J. A. *J. Chem. Phys.* **1972**, *56*, 2257−2261. (b) Hariharan, P. C.; Pople, J. A. *Theor. Chim. Acta* **1973**, *28*, 213−222. (c) Clark, T.; Chandrasekhar, J.; Spitznagel, G. W.; Schleyer, P.; von, R. *J. Comput. Chem.* **1983**, *4*, 294−301. (d) Rassolov, V.; Pople, J. A.; Ratner, M.; Windus, T. L. *J. Chem. Phys.* **1998**, *109*, 1223−1229.
(43) Cancès, M. T.; Mennucci, B.; Tomasi, J. *J. Chem. Phys.* **1997**, *107*, 3032−3041.
(44) Frisch, M. J.; et al. *Gaussian 09*; Gaussian, Inc.: Wallingford, CT, 2010. For a full list of authors, see the Supporting Information.